# A New Method of Introducing Long Range Residual Stresses to Study Creep Crack Initiation

**A. M. Shirahatti*, Y. Wang, C. E. Truman, D. J. Smith**

[1] Solid Mechanics Group, Department of Mechanical Engineering
University of Bristol, Bristol BS8 1TR, United Kingdom
* Corresponding author: anil.shirahatti@bristol.ac.uk

**Abstract** One of the many challenges in the behaviour of structures is to understand if the presence of residual stress plays an important role in contributing to failure of a structure operating at high temperature. A typical example is the reheat cracking, associated with the austenitic stainless steel welded components, where the presence of residual stress is seen as a major factor. A review of previous methods that introduce residual stresses into specimen indicated that a method that doesn't introduce microstructural changes during the generation of residual stresses should be sought. The purpose of this paper is to describe a new method of introducing long range residual stresses at high temperature. The method uses a three bar structure with an initial misfit introduced into the central bar to represent a long range residual stress. The rig was designed so that the induced residual stresses could be characterised easily without using time consuming residual stress measurement techniques. Initial results demonstrated that the magnitude and the interaction of the residual stress with the applied loading is a function of the initial misfit displacements and the relative stiffness of the components of the system. Additionally, the subsequent behaviour of the system, with and without the application of additional loading, is governed by (a) the degree to which the misfit is accommodated by plastic and creep strain and (b) the elastic follow-up provided by the system. The paper describes the design of a test rig and laboratory tests conducted to validate the method.

**Keywords** Residual stress, Creep, Elastic follow-up, 316H stainless steel

## 1. Introduction

Residual stress plays an important role in the component life assessment of the structures. Such stresses may arise usually as a consequence of the manufacturing process and final fabrication. Welding is a typical manufacturing process where, unless the component is subjected to post-weld heat treatment, the residual stress can attain a value close to or equal to the yield stress. Fabrication can also lead to additional locked-in stresses developed from the fitting-up of the different parts of an assembly [1]. Residual stresses are usually treated as secondary stresses. However, in certain circumstances they must be classed as primary. For example, in a cracked structure where the fit-up residual stresses do not self-equilibrate across a ligament, the residual stresses may provide a significant contribution to the plastic collapse of the ligament. Whether they do or not depends on how the residual forces change as a crack grows and plastic deformation accumulates in the structure. This in turn depends on the level of elastic follow-up (EFU). A typical practical case where we expect to see the effect of EFU is shown in fig 1 for a pressurized piping system. As shown schematically, the system and its welds can be treated as a series of springs with the pipe having stiffness K1, K3 and the weld with stiffness K2. When the pipe is built-in and welded we would expect that long range residual stresses to be present and are represented as an initial far field displacement X. The pipe will also be subjected to internal pressure and consequently the system is also subjected to external load P. Elastic follow-up is expected when part of a structure (the area around the welds) reduces its stiffness (either through creation of plasticity and/or the growth of crack) relative (i.e. EFU) to the surrounding material. This would result in additional strain accumulation and relaxation of the initial stresses created during the welding and fit-up.

Many methods have been proposed to generate well defined residual stress fields in laboratory test specimens. In the context of investigating the influence of residual stress on creep, the following

methods have been developed: pre-compression [2-6], quenching [7], side punching [8], Borland specimens [9], ring-weld specimens [10] and electron beam (EB) welding [1, 11, 12]. These methods produce either long-range or short-range residual stress fields. Quenching, Borland specimens and ring welding methods result in specimens with a residual stress field throughout the entire volume. On the other hand, side punching, in-plane compression and EB welding methods result in a residual stress field being set up in a very localised part of the specimen. The second group of methods rely on local, rather than global, incompatible displacements to set up the residual stress field.

Another important observation is that the in-plane compression and EB welded specimens require the introduction of a sharp notch by for example electro-discharge machining, prior to creep testing. Introducing such a notch redistributes the residual stresses and so, care must be taken to ensure that the required levels of residual stress remain in the specimen after this redistribution. Consider the in-plane compression method as an example. Here, a volume of material local to the semi-circular stress raiser deforms plastically and this plastic zone resists the relaxation of the surrounding material. If a long notch is introduced such that it extends through the plastic zone and into the surrounding elastic zone then the elastic zone is free to relax and the residual stress field is lost [11].

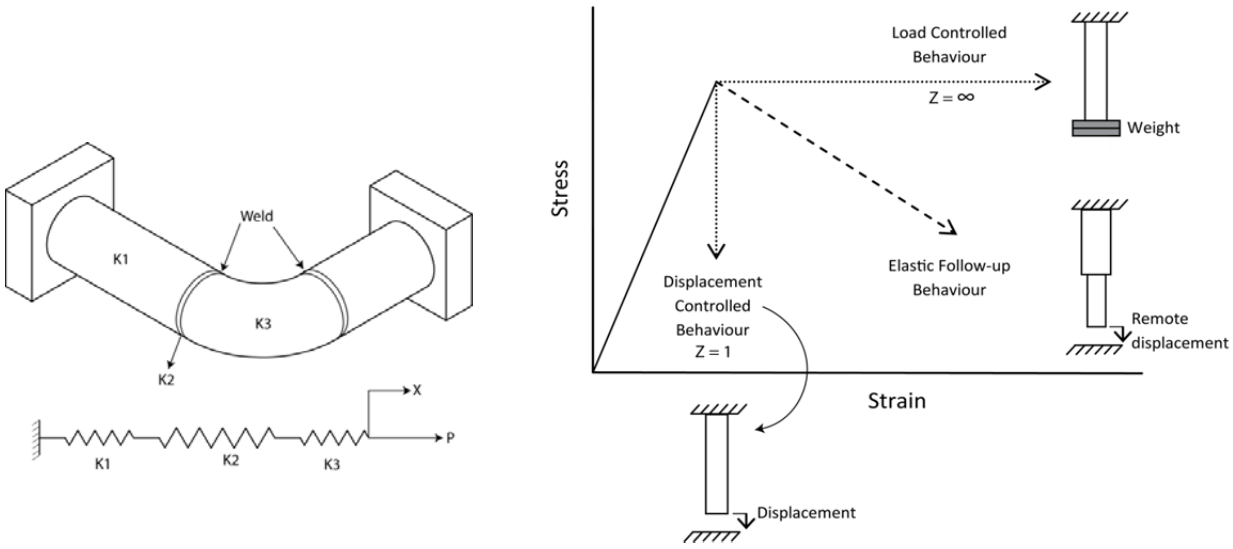


(a) (b)

Figure 1. (a) Built-in welded pipe bend (P is load, X is displacement) (b) Stress-strain behaviour of a local volume

In all the above methods the magnitude and distribution of residual stress are found by time consuming methods i.e. neutron diffraction. Also, in all the cases various and nominally identical specimens are manufactured to determine the stress distribution. For example in case of cylinder quenching by Hossain [7], three specimens were manufactured and the neutron diffraction method was used to measure the stress distribution after quenching, short term ageing (1.25 hrs) and long term ageing (1800 hrs). In all of the above methods, residual stress is introduced at room temperature and when the specimen is subjected to high temperature the magnitude of residual stress is reduced drastically (≈30% reduction) [2-8] due to the lower yield strength at high temperature. In all the cases, the residual stress at high temperature was determined using finite element analysis.

In order to study the effect of residual stress, it is desirable that the method chosen to induce residual stress in the specimen causes no other changes which might influence creep. It is also desirable that residual stress fields set up in the laboratory creep specimens are representative of the long range residual stress fields found in engineering structures.

Of the various methods reviewed only side punching, in-plane compression and EB welding have been used to study the effect of residual stress and applied load on creep under load control conditions. These techniques can also be used to carry out displacement controlled tests. In practical circumstances relaxation of residual stress in one section is compensated by changes in residual stress distribution in other sections to keep the complete structure in equilibrium, i.e. components are often subjected to combined displacement and load controlled situations as shown in fig 1b. It is not possible to study this effect using the reviewed samples and techniques.

A new method is presented that introduces residual stress in a controlled manner such that the stress can be calculated easily at any time and without the use of time consuming residual stress measurement techniques.

## 2. Three bar structure

The new method is based on a classical three bar model and is developed to introduce long range residual stresses through strain incompatibility. This model (or system) has several key features relevant to the high temperature problems of creep crack initiation and growth. The magnitude and the interaction of the residual stress with the applied loading are a function of the initial misfit displacements and the relative stiffness of the components of the system. The subsequent behaviour of the system, with and without the application of additional loading, is governed (a) by the degree to which the misfit is accommodated by plastic and creep strain and (b) the elastic follow-up provided by the system.

### 2.1. Model

Figure 2 shows the three bar structure model consisting of two outer bars ‘B’ and a central bar combination of bar ‘A’ and a compact tension, C(T) specimen. The bars A and B are able to deform elastically and have stiffness $K_{in}$ and $K_{out}$ respectively. An initial misfit, ‘X’ exists between the bars so that joining the bars together introduces fit-up residual stresses into the system, with tension in bar A and balancing compression in bar B. The residual force in the middle bar does not self equilibrate across a section but the tensile residual force in middle bar is in equilibrium with the net compressive force in the outer bars. The structure can be subjected to the applied load ‘P’ so that when plasticity, creep or crack growth occurs in the C(T) specimen and the overall EFU factor, Z is given by

$$Z = Z_{eff} Z_s \tag{1}$$

where,
$$Z_{eff} = \left(\frac{1+\alpha_{eff}}{\alpha_{eff}}\right) \text{ and } Z_s = \left(\frac{1+\beta}{\beta}\right)$$

$$\beta = \frac{K_{in}}{K_s}\ , \quad \frac{1}{\mathrm{K_{eff}}} = \frac{1}{\mathrm{K_S}} + \frac{1}{\mathrm{K_{in}}}\ , \quad \alpha_{eff} = \frac{2K_{out}}{K_{eff}} \tag{2}$$

and $K_s$ is the stiffness of the specimen.

A detailed derivation of this is given in [13]. Figure 3 shows the overall elastic follow-up factor as a function of relative effective stiffness ratio. When the elastic follow-up factor is in excess of 6 (or 1/Z=0.167) these conditions essentially correspond to load controlled conditions, where as an elastic follow-up factor of more than 1.25 (or 1/Z=0.8), represents displacement controlled conditions.

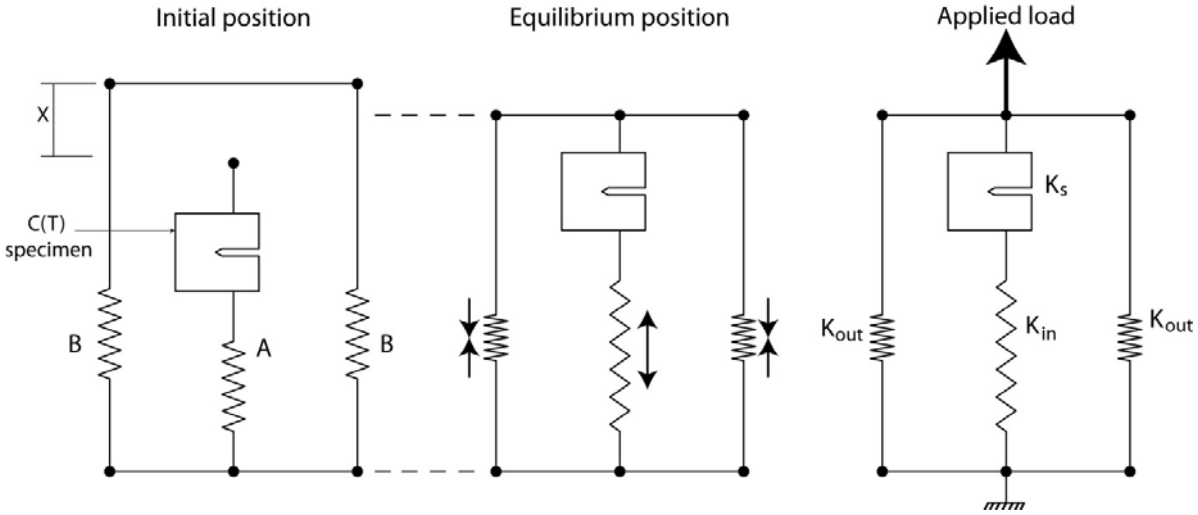


Figure 2. Three bar structure

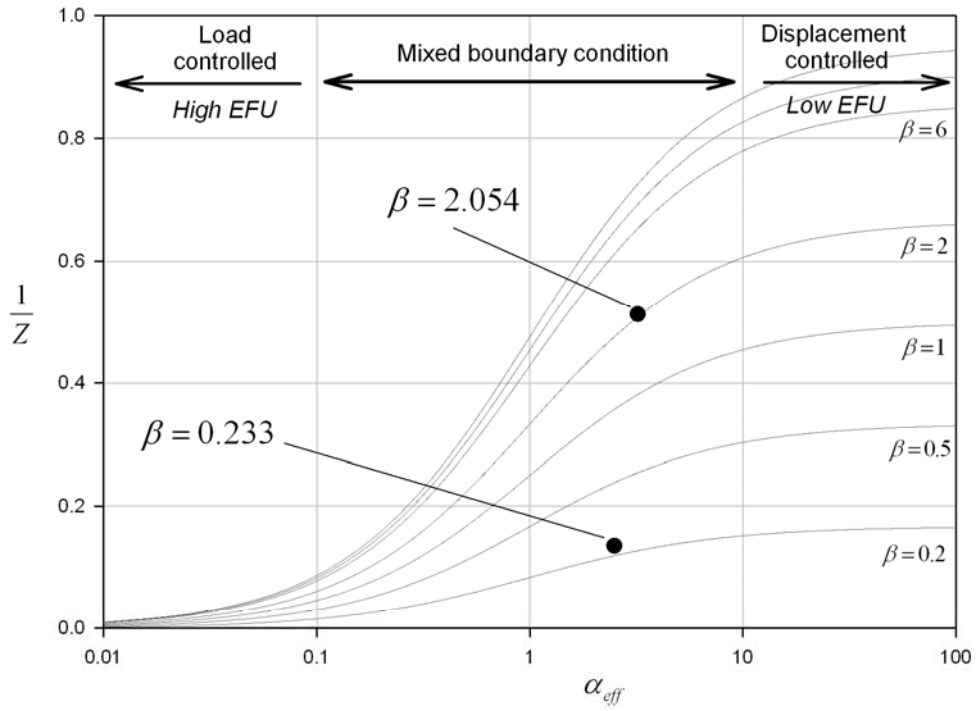


| Overall EFU Z | 1/Z | β | Diameter of bar (mm) | | Overall length (mm) |
|---|---|---|---|---|---|
| | | | Middle | Side | |
| 1.86 | 0.538 | 2.054 | 25.4 | 19.05 | 714 |
| 6.61 | 0.151 | 0.233 | 10 | 10 | 864 |

Figure 3. Variation of overall EFU with effective stiffness ratio in three bar structure

### 2.2. Behavior of the structure with applied load

Figure 4 shows loading conditions and relaxation during plasticity for a representative three bar structure. AA' gives the initial misfit, OB and OB' give the residual force in middle and outer bars respectively. When the structure is further subjected to external load, the force in the middle bar increases from B to C. At point C yielding of specimen starts and the specimen takes no further load and follows line CD while outer bar remains in the elastic range and follows path A'D'. Until yielding at point C, the initially induced residual force remains constant in the middle and outer bars and follows paths B-1 and B'1' respectively. As the applied load increases and the amount of plastic deformation in the specimen becomes equal to the initial misfit, the residual force reduces to zero. The rate of residual force relaxation for a mixed boundary condition follows path 1-2. The gradient of relaxation curves (1-3,1-2 or 1-4) depend upon the elastic follow-up factor. Structures having high EFU will follow path 1-4 while low EFU structures will follow path 1-3. Hence, the influence of initial residual stress present in a structure is dependent on the associated level of EFU.

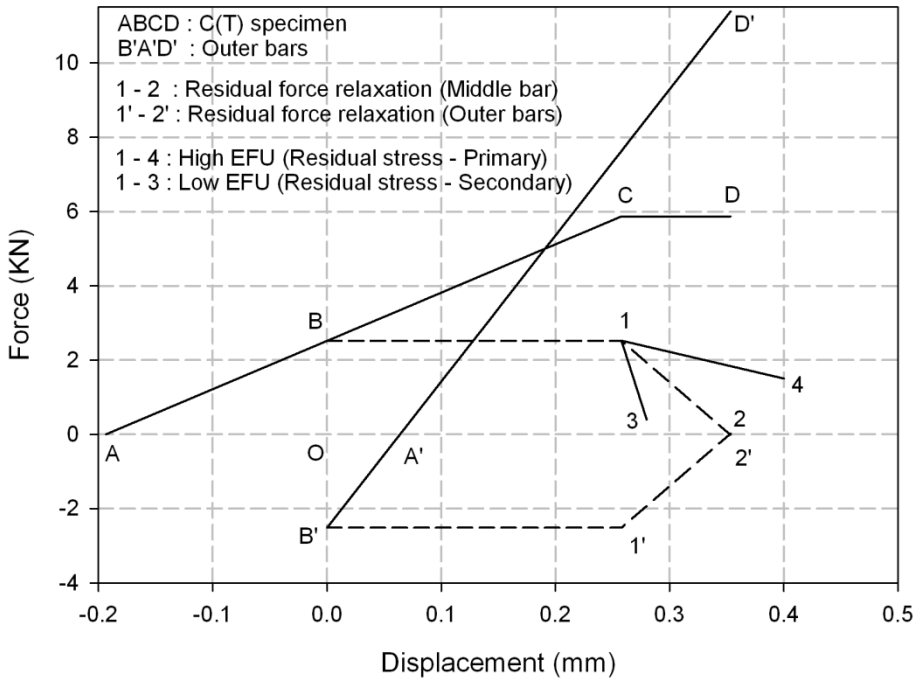


Figure 4. Loading and subsequent relaxation of a three bar

## 3. Experimental studies

### 3.1. Design of test rig

An experimental three bar test rig was designed based on the conceptual model discussed in the earlier section. Since the design was centered around a conventional cylindrical furnace with a maximum internal diameter of 130 mm for a creep test frame, the design was constrained to the available maximum diameter of the furnace, the overall length of the structure (1000 mm), the ease of assembly, the ability to introduce known residual stress at high temperature and then to apply a predetermined load to the assembly. The overall arrangement of the test rig is shown in fig 5 and the material properties of the components for the test rig are tabulated in table 1. The middle bar was a combination of 316H stainless steel C(T) specimen and a Nimonic bar of diameter 25.4 mm while the side bars were Nimonic bars of diameter 19.05 mm. These dimensions are selected to provide an EFU value of about 2 (as shown in fig 3). All bars were screwed to a top and bottom end piece

made from EN24T steel. Two linear voltage displacement transducers (LVDT) were mounted on each side of the upper and lower end to measure the total displacement of the structure. Also, two additional LVDTs were connected to the C(T) specimen to measure load line displacement. Four high temperature strain gauges (ZFLA-3-11) were mounted on the middle and side bars at $90^0$ intervals to measure the residual force. In total seven thermocouples (3-specimen, 1-room, 3-strain gauge) were connected to measure the specimen temperature, room temperature and temperature at the point of application of strain gauges. A direct current potential drop (PD) system was connected to the C(T) specimen to measure crack initiation and growth. The overall arrangement was fitted into a creep test rig so that an external load was applied to the assembly via a lever arm arrangement.

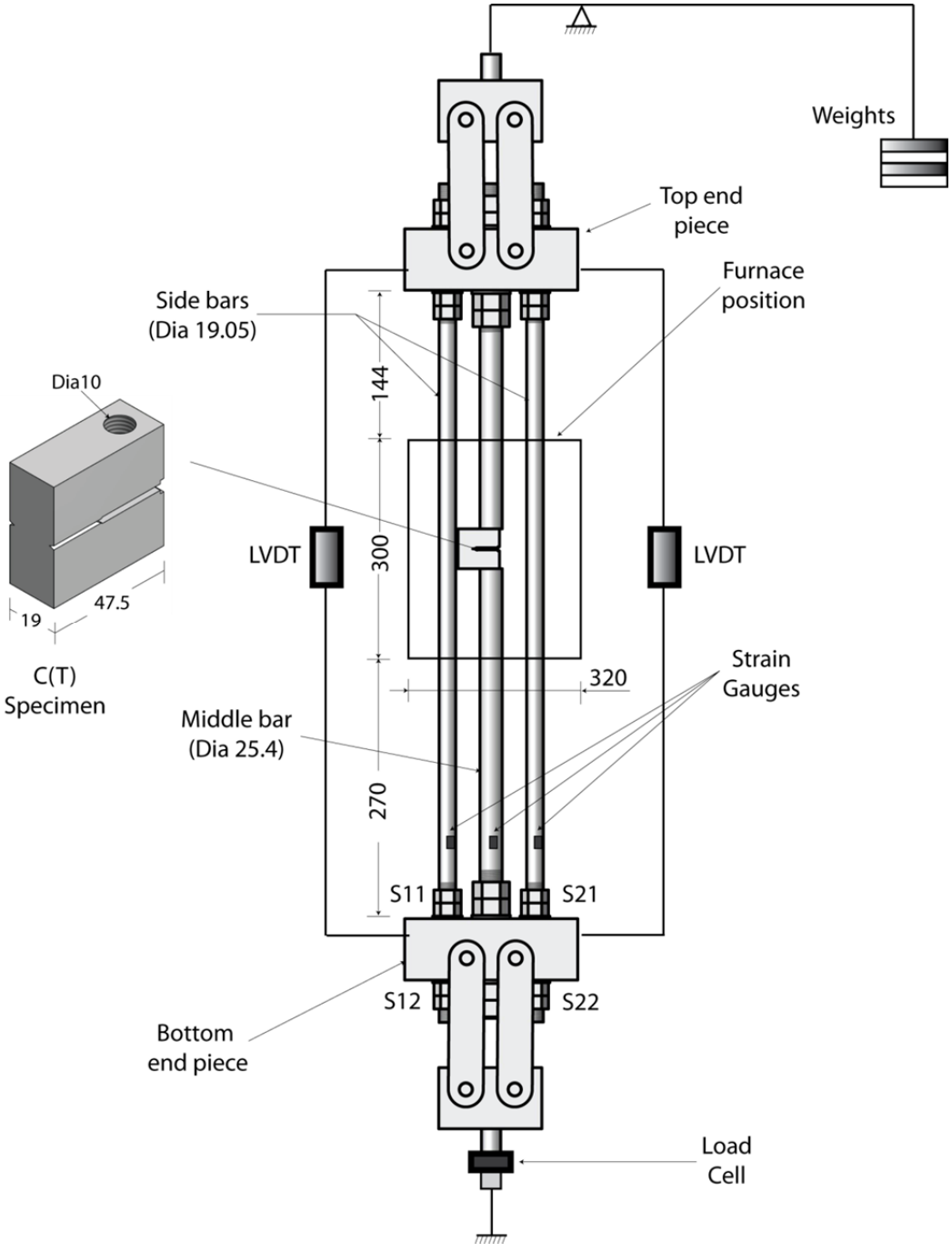


Figure 5. Three bar test rig (All dimensions in mm)

### 3.2. Calibration tests

A series of calibration tests were conducted and divided into two categories; preliminary tests and an load-unload test. Tests were carried out at high temperature and using a 316H stainless steel C(T) specimen. The C(T) specimen was manufactured as per ASTM 1457 but using a screw fitting arrangement rather than pins to load the specimen. This was adopted to ensure accurate measurement of stiffness rather than conventional pin loading. To restrict the crack growth, a 1 mm diameter hole was introduced at the end of standard 0.1 mm wide EDM notch.

Preliminary tests were conducted to determine the stiffness of bars, specimen and determine the overall elastic follow-up value for the rig experimentally. Two applied load tests, within the elastic region, were conducted such that in each case the temperature of the C(T) specimen was maintained at $550^0$C. In the first test only the middle bar with the C(T) specimen was connected to both end pieces. In the second test both the side bars are connected to the top and bottom end bars but the middle bar with C(T) specimen was connected only to the top end piece such that it was free to move (i.e. used to record the C(T) specimen temperature). In each case, the load cell, the temperature at different locations, strain gauge, total displacement and CMOD were measured. The results from these tests are discussed later.

The second category of test was a load-unload test undertaken to understand the relaxation of residual force with applied load. First, a residual stress was introduced into the structure. The middle bar with the C(T) specimen was connected to both end pieces. Side bars were connected to only the top end piece and were free to move through the clearance holes in the bottom end piece. All instruments were then connected to the test rig and the furnace was heated to achieve 550 $^0$C for the C(T) specimen. This arrangement permitted free thermal expansion of the bars and the specimen. When a stable temperature was achieved, nuts S11 and S21 (shown in fig 5) were screwed down, so that the top and bottom end pieces were forced apart. This resulted in the middle bar loaded in tension and the side bars carried the balancing compressive forces. The force in each bar was determined via the strain gauges. Finally when the desired residual force was introduced into the structure, nuts S12 and S22 on side bars were fixed. Having introduced the desired residual stress into the C(T) specimen, the entire assembly was repeatedly loaded and unloaded to progressively higher load levels. The residual force in all three bars, load line displacement of C(T) specimen, potential drop readings and overall extension of the rig were recorded for both load and unload path.

Table 1. Properties of materials for three bar structure

| Material | Young's Modulus (GPa) | Yield Strength (MPa) | Tensile Strength (MPa) |
|---|---|---|---|
| 316H stainless steel at $550^0$C | 151 | 172 | 444 |
| Nimonic 80A at $550^0$C | 187 | 875 | 1210 |
| EN24T Steel at room temperature | 210 | 680 | 925 |

Table 2. Comparison of theoretical and experimental values

| | $K_s$ N/mm | $K_{in}$ N/mm | $K_{out}$ N/mm | $K_{eff}$ N/mm | B | $\alpha_{eff}$ | $Z_s$ | $Z_{eff}$ | Z |
|---|---|---|---|---|---|---|---|---|---|
| Theoretical | 69696 | 155047 | 85139 | 48083 | 2.23 | 3.54 | 1.45 | 1.28 | 1.86 |
| Experimental | 75781 | 155647 | 81761 | 50967 | 2.05 | 3.21 | 1.48 | 1.31 | 1.95 |

## 4. Results and discussion

The theoretical value of the overall elastic follow-up of the rig was calculated using the equations provided in [13]. Results from the preliminary tests consisted of measured strains, applied load, CMOD, overall displacement of the rig, accurate measurement of the diameters and length of the bars. The initial tensile tests measured the stiffness for each element of the assembly. Table 2 compares the experimental values obtained from preliminary test with theoretical values. It is evident from the results that a good agreement was found.

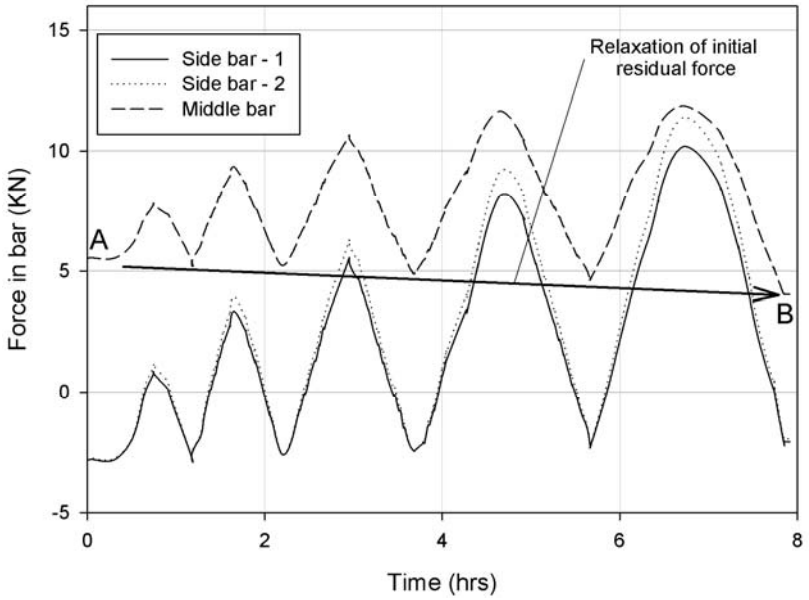


Figure 6. Variation of force in all bars with time

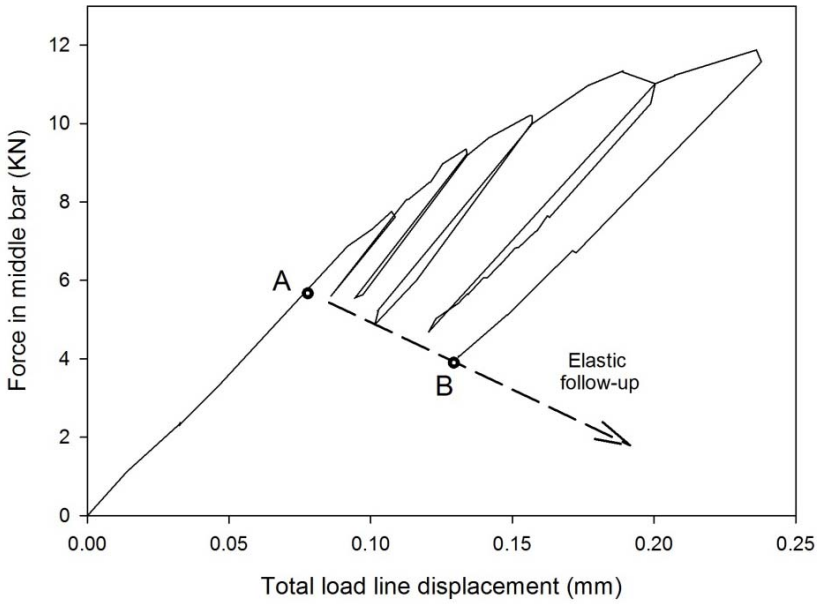


Figure 7. Load versus total load line displacement for C(T) specimen

The test results from the second category of tests are shown in fig 6, and give the details of variation of the residual force and its relaxation as the applied load increased. It is observed that under equilibrium condition, the total compressive residual force in the side bars was approximately equal

to the tensile residual force in middle bar. During the cyclic loading process, the tensile residual force in middle bar relaxed from 5.65 KN to 3.8 KN while the compressive residual force in the side bars relaxed from 2.8 KN and 1.9 KN.

Figure 7 shows the load acting on C(T) specimen against total load line displacement measured during the cyclic loading phase of the test. The following points should be noted. First at point 'A' the C(T) specimen was subjected to a tensile load of 5.65 KN while the total load applied to the assembly was zero. This tensile load corresponds to the initial level of preload in the assembly at the start of the cyclic loading phase of the test.

Second, five unloading lines did not return to the CMOD point 'A' from which the test started. This was due to the accumulation of plastic deformation in the specimen. It can be seen that about 0.06 mm of plastic CMOD had accumulated at the final unloading step. Also, the gradient of each of the unloading lines remained constant. This shows there has been no crack growth during cyclic loading and the same was recorded by PD system.

Third, the line AB corresponds to the locus of unloaded points and reveals that the initial preload relaxed, as plastic deformation accumulated in the specimen thereby reducing the misfit. At point B, with an applied load of zero, the 3.8 KN load on the C(T) specimen corresponds to the level of preload remaining in the assembly i.e. 33% reduction in the initial preload level. An important feature of the behaviour of this assembly is that the relaxation line AB has a slope dependent on the relative stiffness of the assembly and in turn corresponded to the EFU associated with the structure. To achieve different values of EFU, different combinations of diameters of the middle and the side bars can be used. For example, in the present rig if the dimensions are changed so that the middle and side bars diameter is 10 mm and overall height is 864 mm, one can achieve overall EFU of 6.61 (1/Z=0.151) as shown in fig 3.

## 5. Concluding remarks

Four methods of inducing residual stress in laboratory creep specimens were reviewed. These include quenching, side punching, in-plane compression and welding methods. It was found that the ability of these methods to provide insight into the effect of residual stress on creep in engineering structures is limited. These methods cause micro-structural changes to the material as well as inducing residual stress. Also, the short-range residual stresses produced by some of the methods do not accurately represent the long-range residual stresses found in many engineering structures. In each of these methods residual stress measured at room temperature before the start of test will change when the specimen is subjected to high temperature. None of the methods determine the effect of residual stress on creep and complete structure when the residual stress relaxes. We therefore conclude that new methods which can induce long-range residual stress without causing micro-structural change in the material and can represent combine boundary condition are required.

A new method based on a three bar structure illustrated that residual stresses can be induced into a specimen at high temperature in a controlled manner and can be characterised easily without the use of time consuming measurement techniques. The proposed method does not cause any micro-structural change in the specimen and provides details of residual stresses distribution in complete structure at any time. Calibration tests revealed that the structure replicates mixed boundary conditions. Different combinations of diameters of the middle and side bars can be used to achieve different elastic follow-up factors and can therefore study the influence of EFU on initial residual stress and structure as a whole. The new method and the test rig designed can be used for both cracked and uncracked specimens to carry out short and long term creep tests.

## Acknowledgements

The authors gratefully acknowledge EDF Energy Limited for providing financial support for this work.

## References

[1] P. Kapadia, C. M. Davies, D. W. Dean, and K. M. Nikbin, Numerical simulation of residual stresses induced in compact tension specimens using electron beam welding, in Proceedings of the ASME 2012 Pressure Vessels & Piping Conference, July 15-19, 2012, Toronto, Ontario, Canada.

[2] M. Turski, High temperature creep cavitation cracking under the action of residual stress in 316H stainless steel. PhD thesis, University of Manchester, UK, 2004.

[3] N. P. ODowd, K. M. Nikbin, R. C. Wimpory, F. R. Biglari, and M. P. ODonnell, Computational and experimental studies of high temperature crack initiation in the presence of residual stress, Journal of Pressure Vessel of Technology, vol. 130, pp. 0414031–0414037, 2008.

[4] N. P. ODowd, K. M. Nikbin, R. C. Wimpory, and F. R. Biglari, Creep crack initiation in a weld steels: Effects of residual stress, in Proceedings of Pressure Vessels & Piping Conference, PVP2005, July 17-21, 2005, Denver, Colorado USA.

[5] S. Kamel, C. Davies, H. Lee, and K. Nikbin, Effect of crack extension in a compact tension C(t) specimen containing a residual stress on the stress intensity factors, in Proceedings of the ASME 2010 Pressure Vessels & Piping Conference, PVP2010, July 18-22, 2010, Bellevue, Washington, USA.

[6] H. Y. Nezhad, N. P. ODowd, C. M. Davies, K. M. Nikbin, and R. C. Wimpory, Study of creep relaxation behaviour of 316h austenitic steels under mechanically induced residual stress, in Proceedings of the ASME 2011 Pressure Vessels & Piping Conference, PVP2011, July 17-21, 2011, Baltimore, Maryland, USA.

[7] S. Hossain, Residual stresses under conditions of high triaxiality. PhD thesis, University of Bristol, UK, 2005.

[8] S. Hossain, C. E. Truman, and D. J. Smith, Generation of residual stress and plastic strain in a fracture mechanics specimen to study the formation of creep damage in type 316 stainless steel, Fatigue & Fracture of Engineering Materials & Structures, vol. 34, pp. 654–666, 2011.

[9] M. W. Spindler, The use of borland specimens to reproduce reheat cracking in type 316H, Tech. rep., British Energy Generation Ltd., Report No. EPD/AGR/REP/0618/99 Issue 1, Feb 2000.

[10] R. J. Dennis, Detailed analysis of ring-weld creep test specimen, Tech. rep., British Energy Generation Ltd., Report No. BBGB/007/01 Issue 1, Feb 2008.

[11] C. M. Davies, R. C. Wimpory, D. W. Dean, G. Webster, and K. M. Nikbin, Effect of residual stresses on crack growth in 316h steel weldments, 3rd International Conference on Integrity of High Temperature Welds, pp. 333–344, 24-26 April 2007.

[12] C. M. Davies, D. Hughes, R. C. Wimpory, D. W. Dean, and K. M. Nikbin, Measurements of residual stresses in 316 stainless steel weldments, in Proceedings of the ASME 2010 Pressure Vessels & Piping Conference, PVP2010, July 18-22, 2010, Bellevue, Washington, USA.

[13] D. J. Smith, J. McFadden, S. Hadidimoud, A. J. Smith, A. J. Stormonth Darling, and A. A. Aziz, Elastic follow-up and relaxation of residual stresses, Proceedings of the Institution of Mechanical Engineers Part C: Journal of Mechanical Engineering Science, vol. 224, pp. 777–787, 2010.